ATMOSPHERIC FLOW INDICES AND INTERANNUAL GREAT SALT LAKE VARIABILITY

By Young-Il Moon[1] and Upmanu Lall,[2] Member, ASCE

ABSTRACT: This paper identifies connections between the time variability of the volume of the Great Salt Lake (GSL), Utah, and selected atmospheric circulation indices. The indices considered are the Southern Oscillation Index (SOI), the Pacific/North America (PNA) climatic pattern, and the Central North Pacific (CNP) index. We focus on interannual time scales. Low-frequency (interannual or interdecadal) relationships between the Great Salt Lake (GSL) volume change and atmospheric circulation indices are of importance because of their significance for the understanding and prediction of the GSL volume. We use Singular Spectral Analysis (SSA), Multichannel Singular Spectral Analysis (MSSA), and Multitaper Spectral Analysis [or Multitaper Method (MTM)], to identify persistent or nearly periodic patterns in time in each series. MSSA examines the joint modes of variability across the time series, while SSA decomposes each series into its component time patterns. MTM is used for identification of peaks and frequency band structure.

INTRODUCTION

A purpose of the present paper is to understand the role of atmospheric variability in the time behavior of the Great Salt Lake (GSL), Utah, and to examine low frequency relationships between the GSL volume (Fig. 1) and selected atmospheric indices. Global climatic variations lead to hydrologic imbalances with severe impacts in the arid western United States. Variations of regional climate are important for hydrologic extremes such as floods and droughts.

Closed basin lakes are an excellent laboratory for developing an understanding of hydroclimatic interactions in arid regions. They integrate the basin's hydrologic response and represent it over a variety of time scales through their level, salinity, and sediments. The GSL of Utah is a closed lake in the Great Basin, in the arid western United States. Usually, closed lakes are in arid regions of the world where the long-term average evaporation rate exceeds the average precipitation. The only outlet from the lake is evaporation from its surface. The inflow is from precipitation on the lake and runoff which is induced by precipitation in the drainage basin. The water entering the lake consists mainly of inflow from the Bear, Weber, and Jordan Rivers, and other smaller surface streams. Precipitation adds about half as much as the surface inflow, while direct ground-water inflow contributes a small amount of water. However, many of the influent streams are maintained by ground-water recharge from mountain aquifers. Over historical time, it has shown significant fluctuations in size and surface elevation depending on the prevailing climatic factors such as amount of precipitation and evaporation over its watershed. Fluctuations in lake level range from a high of 1,283.77 m (4211.85 ft) in 1986 and 1987 and to a low of 1277.42 m (4191 ft) in 1963. The lake level rises and falls from 41 cm to 46 cm (16 to 18 in.) each year because maximum inflow occurs during the spring and maximum evaporation takes place in late summer and fall. Wet and dry weather persistence also affect the lake level fluctuations. The GSL is at the lowest part of the basin, approximately 1,280.16 m (4,200 ft) above sea level. Historically, it has fluctuated in area within latitudes 40°20′ and 41°40′ N, and longitudes 111° 52′ and 113° 06′ W. The GSL is approximately 113 km (70 mi) long and 48 km (30 mi) wide, with a maximum depth of 13.1 m (43 ft) [average depth 5.0 m (16.5 ft)]. The large surface area and shallow depth make the lake very sensitive to fluctuations in long-term climatic variability.

The impact of climate variability on the hydrologic cycle is of importance from the point of view of understanding the underlying dynamics of the hydrologic system. The regional climate is governed primarily by topography, vegetal cover, geomorphological characteristics, and the large-scale atmospheric circulation. The climate is strongly affected by the nature of temporal variations in atmospheric circulation. Lorenz (1990) argued that longer period variations are frequently looked upon as change in climate. The ability to establish a low-frequency relationship between the Great Salt Lake and atmospheric circulation patterns is thus important for an understanding of connections between long-term climatic and lake volume changes.

Barnston and Livezey (1987) identified some relations between patterns of Northern Hemisphere 700-mb circulation and regional streamflow in United States. They identified five seasonal large-scale climatic patterns that represent the core climate responsible for the forcing of regional streamflow variability. They are the Pacific/North American (PNA), Mixed Pacific (MP), Asian/Eurasian (AE), East Pacific (EP), and North Atlantic (NA) patterns. They demonstrated that regional streamflow response to these forcing regimes varies from month to month. The PNA pattern is documented by Lins (1993) as a major influence in the GSL region. From the recent work of Trenberth and Shin (1984), Klein and Bloom (1987),

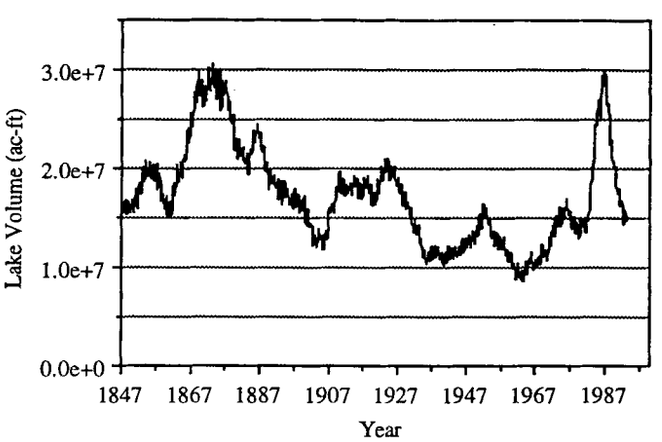

FIG. 1. Variations of Great Salt Lake Volumes from 1847 to 1993

[1]Res. Assoc., Utah Water Res., Utah State Univ., Logan, UT 84322-8200.

[2]Prof., Utah Water Res. Lab., Utah State Univ., Logan, UT.

Note. Discussion open until September 1, 1996. To extend the closing date one month, a written request must be filed with the ASCE Manager of Journals. The manuscript for this paper was submitted for review and possible publication on February 6, 1995. This paper is part of the ***Journal of Hydrologic Engineering***, Vol. 1, No. 2, April, 1996. ©ASCE, ISSN 1084-0699/96/0002-0055–0062/$4.00 + $.50 per page. Paper No. 10106.

Kiladis and Diaz (1989), Cayan and Peterson (1989), Leathers et al. (1991), and Lins (1993), among numerous others, it is very clear that large-scale atmospheric and oceanic conditions exert considerable influence on the low-frequency (interannual to interdecadal) patterns of North American climatic and hydrologic variability. Klein (1985) and Klein and Boom (1987) provide a comprehensive review of the literature documenting the superiority of 700-mb heights over other climatological variables as indicators. Barnston and Livezey (1987) produced a comprehensive assessment of circulation at the 700-mb level and provided a classification of circulation types for comparison with streamflow. They showed that 700-mb patterns are better predictors of temperature and precipitation than 500-mb patterns. Hirschboeck (1987) showed that there is linkage between anomalous circulation patterns and severe floods in the western, central, and eastern regions of the United States. Cayan and Peterson (1989) found that streamflow fluctuations in the west exhibit significant correlation with the winter season mean sea-level pressure anomaly patterns.

Lall and Mann (1995) analyze the time series of Great Salt Lake (GSL) monthly volume change, monthly precipitation, temperature, and streamflow by using Singular Spectral Analysis (SSA) and Multitaper Spectral Analysis. They showed signals with periods of approximately 15–18, 10–12, 3–7, and 2 years that seem to be consistent across time series. Mann et al. (1995) present connections between the GSL volume and large-scale climate variations through an analysis of the time series of the Great Salt Lake monthly volume change, monthly precipitation and streamflow, and gridded U.S. sea-level pressure and global temperature data. They isolated decadal and secular modes of climate variability that are coherent with volume change variations.

Here, monthly lake volume change data have been analyzed to identify patterns at interannual time scales. This paper uses Singular Spectrum Analysis (SSA), Multichannel Singular Spectrum Analysis (MSSA), and the Multitaper method (MTM) to coanalyze the time series of lake volume and atmospheric circulation indices. SSA is used to analyze the time series of GSL and atmospheric indices. SSA gives a trend and oscillatory modes separated from the "noise." We used MSSA to identify coherent temporal patterns common to GSL and atmospheric indices. A significance testing of spectral peaks was done using the MTM procedure. These analyses show common modes in 5, 3.4, 2.4, 2.2, and 1 year frequency bands. The periodicity near 2 years may be from QuasiBiennial Oscillation (QBO), which is observed in the equatorial stratospheric winds. Trenberth and Shin (1984) showed QBO in sea-level pressures over the Northern Hemisphere. Periodicities in the 3 to 5 year range may be related to the El Niño–Southern Oscillation (ENSO). Also, the MTM shows low frequency signals longer than 10 years for GSL and atmospheric indices.

We begin with a brief review of the data set used and an introduction to a description of selected methods. Results and conclusions of the research are presented next.

DATA SETS

Four times series are analyzed here. They are the GSL monthly volume change from November 1847 to November 1993, monthly Southern Oscillation Index (SOI) from January 1882 to November 1993, monthly Pacific–North America Index (PNA) from December 1946 to July 1993, and monthly Central North Pacific Index (CNP) from January 1899 to November 1993. Cayan and Peterson (1989) and Cayan and Webb (1992) showed that the indices are significantly correlated with streamflow in the United States. In particular, the impact of variability for atmospheric circulation is strong in the western United States, where water resources are limited.

The Great Salt Lake level data were provided by Scott D. Bartholoma of Utah District, U.S. Geological Survey (USGS) office, and the atmospheric data (SOI, PNA, and CNP) by Daniel R. Cayan of Scripps Institution of Oceanography, University of California–San Diego.

Great Salt Lake

The Great Salt Lake levels were converted to lake volumes from November 1847 to November 1993 using the elevation-volume relationships of the north and south arms (The lake was divided into a north and south arm by the Southern Pacific Causeway completed in 1959–60). These relationships were taken from Sangoyomi (1993) who fitted a second-order polynomial to elevation-volume tabulations available from USGS. We analyze month-to-month volume changes, rather than the volume itself, because they provide a more direct comparison with the atmospheric variables.

Southern Oscillation Index (SOI)

The SOI series consist of time series of normalized monthly mean differences in sea-level pressure (SLP) at Tahiti (approximately 150W, 18S) and Darwin (approximately 130E, 13S) from January 1882 to November 1993.

$$\text{SOI} = \text{SLP(Tahiti)} - \text{SLP(Darwin)} \tag{1}$$

The El Niño–Southern Oscillation is a family of atmospheric and oceanic variations originating in the tropical Pacific Ocean but causing significant perturbations of general atmospheric circulation globally. The ENSO has a typical life cycle of about 3–8 years. When SOI is a low negative value, a strong ENSO warm event develops. The atmospheric pressure in the eastern Pacific decreases and the easterly trade winds weaken. Then, the warm water pool of the western tropical Pacific Ocean usually extends eastward, piling up off the coast of Peru and southern Ecuador. Organized cumulus convection (and thus latent heating of the tropical atmosphere) also shifts eastward causing significant disruptions of the general atmospheric circulation all over the globe.

Perhaps the most important aspect of an ENSO event is the change in the precipitation patterns over the world. There are increases in precipitation over the western United States with a typical ENSO event and drought over the continental United States with a La Niña event (anti–El Niño event) (Ropelewski and Halpert 1987; Keppenne and Ghil 1992).

Pacific North America Index (PNA)

Many authors have demonstrated how the climatic conditions in North America are related to the circulation far afield over the central North Pacific. In particular the precipitation along the Pacific coast of North America is strongly affected by the orientation of the North Pacific storm track (Namias 1978). Sea-level pressure (SLP) has been shown to be an adequate indicator of atmospheric circulation, especially over the extratropical oceans during winter (Emery and Hamilton 1985) and is reasonably well correlated with precipitation over the west coast (Cayan and Roads 1984).

Cayan and Peterson (1989) note that correlations between PNA and December–August mean streamflow anomalies reflect variations in the strength and position of the mean North Pacific storm track entering North America and shifts in the trade winds over the subtropical North Pacific. They show that a region where stream flow is best tuned to the PNA is the northwestern United States. The PNA index (Horel and Wallace 1981) was constructed from monthly 700 mb height anomalies over the December 1946 to July 1993. The PNA is defined by

$$\text{PNA} = H(170\text{W},20\text{N}) - H(165\text{W}),45\text{N}) + H(115\text{W},58\text{N}) - H(90\text{W},30\text{N}) \tag{2}$$

This pattern is almost certainly the single most important determinant of winter season weather for most of the North American continent. Its positive phase is associated with relatively dry long-wave ridges over the western United States. Something resembling a negative PNA phase was shown to be associated with enhanced precipitation in the GSL region on a decadal time scale by Mann et al. (1995).

Central North Pacific Index (CNP)

The CNP index (Cayan and Peterson 1989) was constructed by averaging the SLP (in mb) over the region 35 N–55 N and 170 E–150 W from January 1899 to November 1993. The CNP index is similar to the PNA index, but has the advantage that CNP is available for a longer period than PNA.

$$\text{CNP} = \text{SLP}(170\text{E} - 150\text{W}, 35 - 55\text{N}) \tag{3}$$

METHODS

We use SSA and MSSA to analyze the time series of GSL volume change and atmospheric indices, obtaining trends, separations between a small number of oscillatory modes, and noise. This method has been used in a number of recent climate studies (e.g., Ghil and Vautard 1991; Dettinger and Ghil 1991; Keppenne and Ghil 1992; Vautard et al. 1992; Unal and Ghil, in press 1995; Lall and Mann 1995).

Singular Spectrum Analysis (SSA)

SSA is a Principal Component Analysis (PCA) of the delay coordinates for a time series. Let x_i ($i = 1, \ldots, N$) be a time series. The time series x_i is embedded in an M dimensional space (which has the role of a smoothing window) by forming state vectors from sequences of M consecutive observations; $x_i, x_{i+\tau}, \ldots, x_{i+(M-1)\tau}$ where $i = 1$ to $N - M + 1$, and τ is a sampling rate. The resulting data matrix is denoted by $\mathbf{X}$ with elements $X_{i,j} = x_{i+j-1}$.

The autocovariance matrix of $\mathbf{x}$ (the state vector), $\mathbf{T}_\mathbf{x}$, contains in column j and row i to autocovariance of $\mathbf{x}$ at lag ($i - j$) and represents "patterns" of variability over a window length M. As estimated here, the matrix, $\mathbf{T}_\mathbf{x}$, has a Toeplitz structure which has uniform diagonals and off diagonals, each corresponding to the estimated autocovariance at the corresponding lag.

$$\mathbf{T}_\mathbf{x} = \begin{bmatrix} c(0) & c(1) & c(2) & \cdot & \cdot & \cdot & \cdot & c(M-1) \\ c(1) & c(0) & c(1) & \cdot & \cdot & \cdot & \cdot & \cdot \\ \cdot & c(1) & c(0) & c(1) & \cdot & \cdot & \cdot & \cdot \\ \cdot & \cdot & \cdot & \cdot & \cdot & \cdot & \cdot & \cdot \\ \cdot & \cdot & \cdot & \cdot & \cdot & \cdot & \cdot & \cdot \\ c(M-1) & \cdot & \cdot & \cdot & \cdot & \cdot & c(1) & c(0) \end{bmatrix} \tag{4}$$

where

$$c(j) = \frac{1}{N - \tau j} \sum_{i=1}^{N-\tau j} x_i x_{i+\tau j} \tag{5}$$

The eigendecomposition of the matrix, $\mathbf{T}_\mathbf{x}$, is $\mathbf{E}\Lambda\mathbf{E}^T$, when the eigenvectors $\mathbf{E}^k$ ($1 \le k \le M$) form an optimal basis for describing the series and eigenvalues are λ_k ($1 \le \mathbf{k} \le \mathbf{M}$). Vautard and Ghil (1989) observed that the near-equality of a pair of eigenelements are associated with oscillatory phenomena. Preisendorfer (1988, page 247) showed that the standard deviation ($d\lambda_k$) of estimates of an eigenvalue (λ_k) is $\lambda_k(2/n)^{1/2}$. If ($\lambda_k - \lambda_{k+1}$) is smaller than $d\lambda_k$, the eigenvalues may be considered to be nearly equal. There are a number of techniques for selecting the significant eigenvectors (Preisendorfer 1988). Lall and Mann (1995), first, dropped eigenvectors if the corresponding eigenvalue was smaller than $1/M$ of overall variance, and, second, considered distinct and similar paired eigenvectors only as described. They also checked the significance of their patterns against a white noise hypothesis using rule N with corrections for serial correlation from Preisendorfer (1988, pages 199–206). Rule N is a dominant variance rule. A Monte Carlo simulation with Gaussian data (with and without a specified lag 1 series correlation) is performed to identify the percentiles of the randomly generated eigenvalues of a matrix of dimension equal to the one analyzed by PCA. Denote the 95th percentile for the jth ordered eigenvalue as $\sigma_j(95)$. The number, ns, of significant eigenvalues is a sample is then: ns = No. of $[\lambda_j > \sigma_j(95)]$, $j = 1, \ldots, M$. In this paper, we followed a similar procedure for checking the significance of the eigenvalues for both SSA and MSSA.

We can determine the principal axes (the eigenvectors) of a sequence of M-dimensional vectors through an orthonormal basis (E^k, $1 \le k \le M$).

$$X_{ij} \sum_{k=1}^{M} a_i^k \mathbf{E}_j^k \quad 1 \le j \le M \tag{6}$$

where a_i^k = projection coefficients called the principal components (PCs); the basis vectors $\mathbf{E}^k$ are the empirical orthogonal functions (EOFs) ($1 \le k \le M$); and M = an embedding dimension or window length, which is suggested to be $N/5 \le M \le N/3$ by Vautard et al. (1992). Too small an M leads to smearing of the spectrum and too large an M to splitting of peaks.

If the values of the scalar series are denoted by x_i ($1 \le i \le N$), the equivalent SSA expansion is

$$x_{i+(j-1)\tau} = \sum_{k=1}^{M} a_i^k \mathbf{E}_j^k \quad \text{where } 1 \le j \le M$$

$$\text{and } 1 \le i \le N - M + 1 \tag{7}$$

The kth principal component (PC) is defined as the orthogonal projection of the original series on to the kth EOF.

$$a_i^k = \sum_{k=1}^{M} x_{i+(j-1)\tau+1} \mathbf{E}_j^k \quad 0 \le i \le N - M \tag{8}$$

The PCs are therefore processes of length $N - M + 1$. They can be considered as weighted moving averages or filtered representations of the process x.

SSA is used to isolate the dominant variability or separate the signal that contains a particular frequency band from other signals. Let A be a subset of indices of EOFs and PCs to be used in reconstructing the signal of interest. Vautard et al. (1992) define reconstructed components (RCs) as optimal linear combinations of the corresponding principal components. They represent a filtered (moving average) version of the original data, with a filter defined through the elements of the corresponding eigenvector.

$$(R_A x)_i = \frac{1}{i} \sum_{j=1}^{i} \sum_{k \in A} a_{i-j}^k \mathbf{E}_j^k \quad \text{for } 1 \le i \le M - 1 \tag{9}$$

$$(R_A x)_i = \frac{1}{M} \sum_{j=1}^{M} \sum_{k \in A} a_{i-j}^k \mathbf{E}_j^k \quad \text{for } M \le i \le N - M + 1 \tag{10}$$

$$(R_A x)_i = \frac{1}{N - i + 1} \sum_{j=1-N+M}^{M} \sum_{k \in A} a_{i-j}^k \mathbf{E}_j^k \text{ for } N - M + 2 \le i \le N \tag{11}$$

Multichannel SSA (MSSA)

MSSA (Unal and Ghil, in press, 1995; Vautard et al. 1992) is a Principal Component Analysis in the space and time do-

mains of delay coordinates for several series, often from several sites. This is similar to extended EOF analysis (Weare and Nasstrom 1982). MSSA identifies common and recurring modes of spatial and temporal variation based on the selected embedding dimension M. Here, the "spatial" components are the different time series that are being correlated.

For MSSA, (6) with original L-dimensional data vector $\mathbf{x}_{i,j}$, $1 \leq 1 \leq L$, becomes

$$\mathbf{X}_{i,j} = \sum_{k=1}^{M \cdot L} a_i^k \mathbf{E}_j^k \quad 1 \leq i \leq N - M + 1, 1 \leq j \leq M \cdot L \quad (12)$$

The kth basis vector is an eigenvector of the block-Toeplitz matrix $\mathbf{T}_x$ containing the cross-covariance matrices of the L different channels at lags 0 to $M - 1$. The kth (PCs) and (RCs) are similar to the SSA equations (8)–(11) if we consider an EOF length of $M \cdot L$.

RESULTS

We will first discuss SSA results of GSL monthly volume changes using two different windows and then we show how SSA reconstruction of GSL low-frequency components compares with a 12-month moving average of GSL. We also use Multitaper Method to show coherence between GSL monthly volume change and atmospheric indices. This provides the motivation for a simultaneous decomposition of the time patterns in the GSL monthly volume change and the atmospheric indices. Finally we will present results of MSSA of GSL and three atmospheric indices.

SSA of GSL Monthly Volume Change Using 2 Different Windows

We applied SSA to GSL monthly volume changes with two embedding dimensions of 150 and 600 months, to identify and reconstruct the annual and semiannual cycles from the data. Vautard et al. (1992) show that SSA is typically successful at analyzing periods in the range ($M/5$, M). Consequently we used two different window lengths, $M = 150$ and $M = 600$ to better capture interannual (30–150 months) and interdecadal (120–600 months) signals. The reconstructed annual and semiannual components (RCs) were then subtracted from the raw data. The annual and semiannual cycles explain 74% of the total variance for $M = 150$ while these components account for 71% for $M = 600$, and are quite distinct from the rest. Next, SSA was reapplied to the modified data sets with the annual or semiannual cycles removed.

Pairs of nearly equal eigenvalues identify oscillatory modes for each embedding dimension after removal of the annual or semiannual cycles. These are eigenvalues 5–6 (7.5% and 7.3% of total variance) and 7–8 (6.7% and 6.7%) for $M = 150$ months and 1–2 (8.8% and 8.7%) and 3–4 (8.6% and 8.5%) for $M = 600$ months. The eigenvalues 1–2 and 3–4 for $M = 150$ are not close and appear to represent patterns with duration longer than the window length. Fig. 2(a–b) and (c–d) show the eigenvectors corresponding to the eigenvalues 5–8 ($M = 150$) and 1–4 ($M = 600$) in pairs, respectively. EOFs 5–8 ($M = 150$) show interannual oscillations with a period of approximately 2.5–4 years while EOFs 1–4 ($M = 600$) represent interdecadal oscillations with a period of approximately 12–14 years. The interannual modes (4 years and 2.5 years) are present in the $M = 150$ but not in the $M = 600$ analysis. This is not unexpected given that the second window is not expected to resolve interannual frequencies. The frequencies are identified by a MTM analysis of the RCs for each EOF. The eigenvalues corresponding to these eigenvectors were well above the significance levels indicated by Preisendorfer's rule N with correction for serial correlation. These results are consistent with these reported in Lall and Mann (1995) where SSA

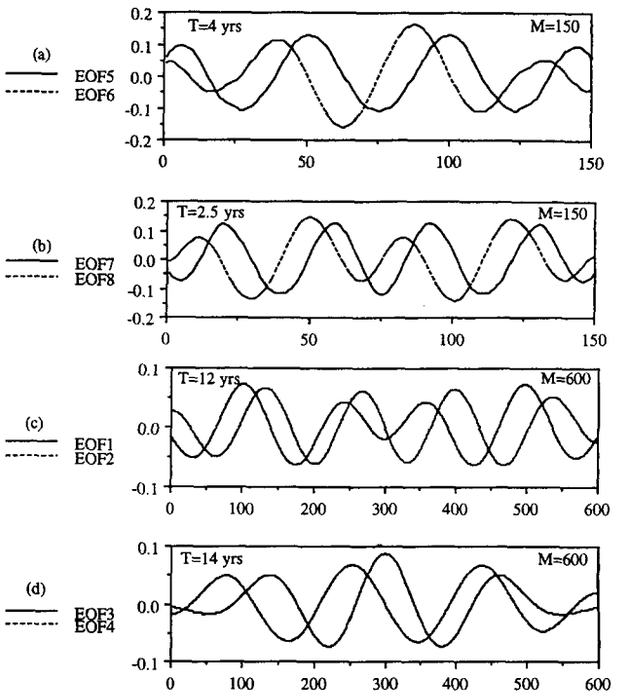

FIG. 2. The Interannual [(a) 4 years; (b) 2.5 years] and Interdecadal [(c)12 years; (d) 14 years] Frequency of Eigenvectors of GSL Monthly Volume Change Using two Different Windows

was used with annual rather than monthly GSL volume change. Ghil and Vautard (1991) and Mann and Park (1993, 1994) also find interdecadal signals with a period around 15–18 years, using slightly longer records of global temperature. The spectral resolution of the different analyses is such that it is not possible to uniquely distinguish between a 12–14 year or 15–18 year cycle, for the record lengths and windowing parameters used.

SSA Reconstructed Low Frequency Components

An interesting aspect of SSA is the detailed reconstruction of any subset K of significant components of the time series. In Fig. 3, SSA reconstructed components of low frequency are computed as a sum of reconstructed components (RCs) corresponding to the pairs of EOFs (Fig. 2), i.e., RC 5 and 6 ($M = 150$) in Fig. 3 is the sum of RC 5 and 6 of $M = 150$. RCs 5–8 with $M = 150$ show interannual oscillations. RC 5 and 6 presents a period of approximately 2.5 years while RC 7 and 8 represents 4 years. RCs 1–4 with $M = 600$ show interdecadal oscillations with a period of approximately 12–14 years. RCs 1 and 2 represent a period of approximately 12 years while RCs 7 and 8 represent 14 years.

Coherence between GSL Volume Change and Atmospheric Indices

The MTM of spectrum analysis (Thompson 1982; Mann and Park 1993) was applied to estimate the coherence between GSL volume change and atmospheric circulation data at selected frequencies. MTM is a nonparametric spectrum analysis method that optimizes the search for spectral peaks. It gives an estimate of the total variance in a window centered at the frequency of interest and aims for improved spectral estimates where the spectrum is mixed, its range is large, the time series is short, and the background "noise" is white. We used the complex multitaper spectral coherence (Vernon et al. 1991), valid for locally white spectral processes to analyze the coherence. Figs. 4, 5, and 6 show the coherence estimated by

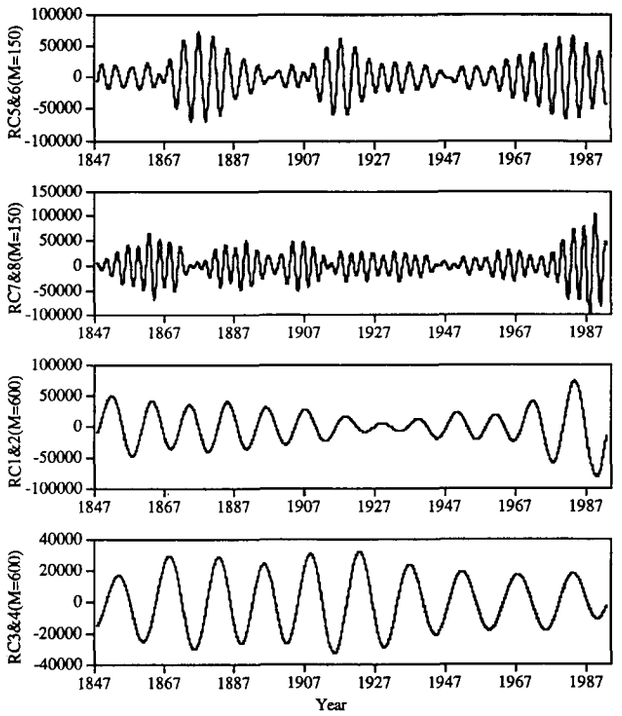

FIG. 3. SSA Reconstructed Components of Low Frequency

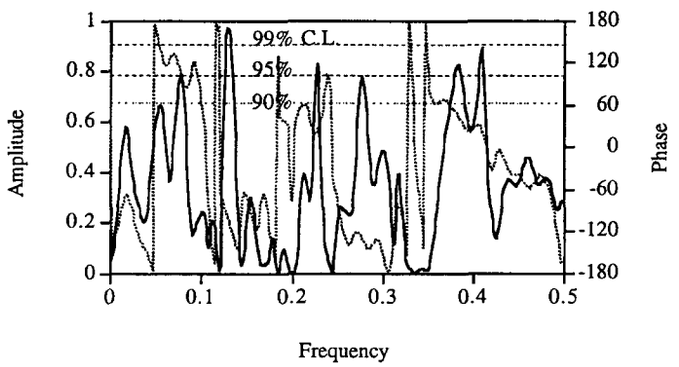

FIG. 4. MTM Coherence (Solid) and Phase (Dots) between GSL Volume Change and SOI, Using Three 2π Tapers and Data from September 1932 to October 1993 [Dashed Horizontal Lines Are 90%, 95%, and 99% Confidence Limits (CLs) for Coherence Amplitude]

MTM (using three 2π tapers) between the GSL volume change and atmospheric circulation data. There is significant coherence between GSL and SOI at 2.4, 2.6, 3.6, 4.4, 7.8, and 12.9 years. PNA and CNP have significant coherence at 2.3 and 3.9 years with GSL.

Note how the phase of each atmospheric index relative to GSL varies by the frequency band of interest. One should focus primarily on the frequency bands with significant coherence, and recall that a phase of 180° is the same as that of −180°. Also, while the PNA and CNP time series represent approximately the same behavior, they are of opposite sign. Consequently, a 90° phase with one should suggest a −90° with the other, as is indeed observed for the 3.9 year frequency band.

MSSA Results

MSSA is applied to the four data sets: GSL monthly volume change, SOI, PNA, and CNP, to see if the joint variation exhibited by these series is consistent with the MTM analyses.

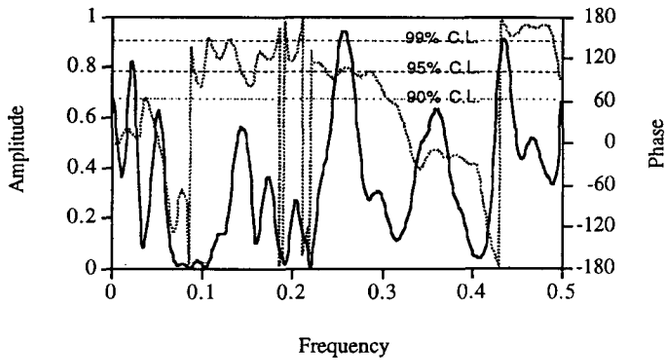

FIG. 5. MTM Coherence (Solid) and Phase (Dots) between GSL Volume Change and PNA, Using Three 2π Tapers and Data from December 1946 to July 1993 [Dashed Horizontal Lines Are 90%, 95%, and 99% Confidence Limits (CLs) for Coherence Amplitude]

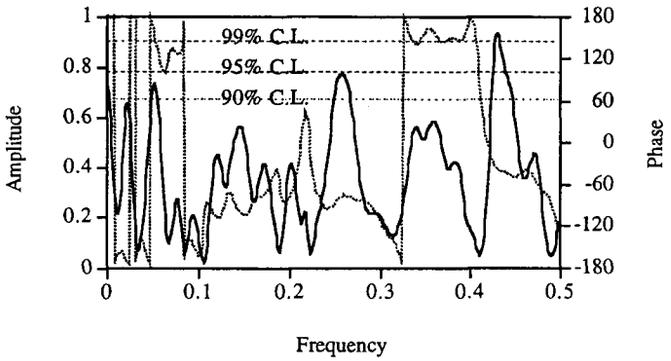

FIG. 6. MTM Coherence (Solid) and Phase (Dots) between GSL Volume Change and CNP, Using Three 2π Tapers and Data from January 1945 to October 1993. Note Consistency in Figs. 5 and 6 Even Though Records of Different Length Are Used. CNP Has Opposite Sign from PNA. Dashed Horizontal Lines Are 90%, 95%, and 99% Confidence Limits (CLs) for Coherence Amplitude]

Because the total data length is 559 months, an embedding of 120 months was used.

Eigenvectors 1 and 2 explained 15.7% of total variance. Eigenvector 3 explained 2.4% and eigenvectors 4–10 explained 12%. Reconstructed components from MSSA corresponding to each data series were analyzed by MTM to identify the frequencies of associated oscillations (significant at the 90% level), if any. Based on this analysis, the first two eigenvectors correspond to annual and seasonal (4 month) cycles [Fig. 7(a)], the third to a secular trend [Fig. 7(b)], and 4–10 to interannual cycles. The eigenvalues corresponding to these eigenvectors were well above the significance levels indicated by Preisendorfer's rule *N* with correction for serial correlation.

Through experimentation with synthetically generated series with approximately the same periodicities as those identified here, we discovered that depending on the number and mix of frequencies across sites, a number of coupled eigenvectors may be needed by MSSA to recover the full set. This observation and significance testing with MTM at different tapers helped reassure us that the set of frequencies identified in RCs 4–10 was meaningful. In summary, we find cycles with periodicities of approximately 2.3, 3, and 5 years that are common to all the four series analyzed. The GSL and the SOI series also show a significant periodicity around 8 years. In addition, the GSL series shows a significant periodicity around 14 years. These periodicities are consistent with the ones identified earlier and by Lall and Mann (1995).

The interannual "signals" in the four series as identified by

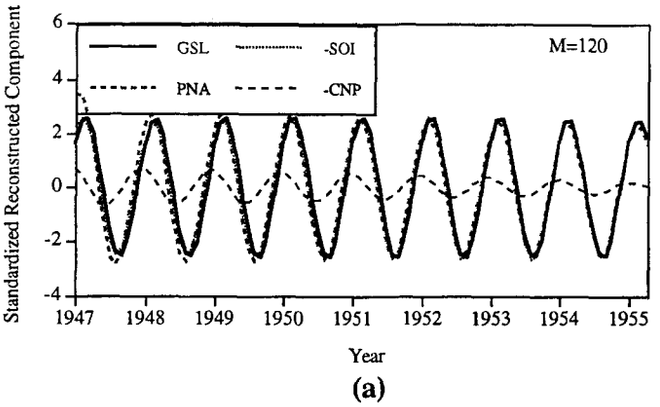

(a)

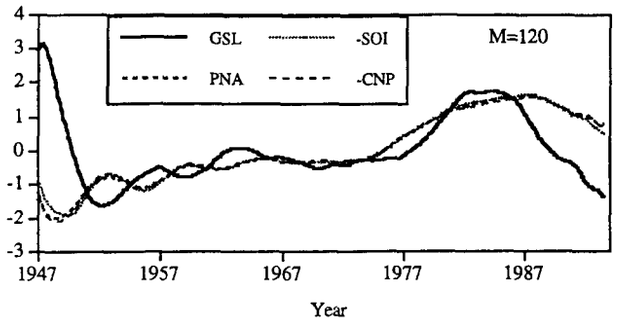

(b)

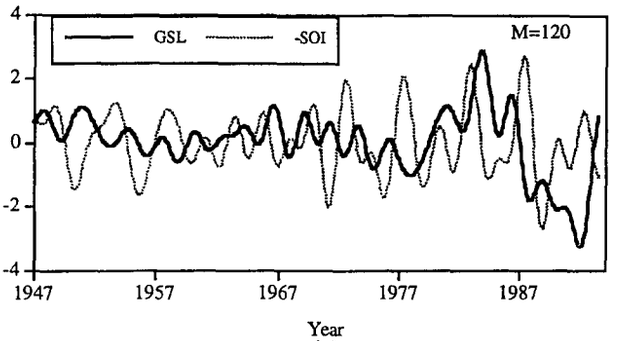

(c)

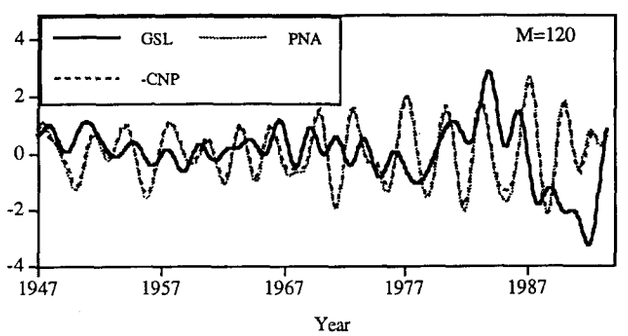

(d)

FIG. 7. MSSA Reconstructed Components: (a) RC 1–2, Showing Annual Cycle (Note That -SOI and -CNP Are Used for Plotting This Figure); (b) RC 3, Showing Secular Trend (Note That -SOI and -CNP Are Used for Plotting This Figure); (c) RC 4–10, Showing Interannual Variations (Note that -SOI is Used for Plotting This Figure); (d) RC 4–10, Showing Interannual Variations (Note that -CNP is Used for Plotting This Figure)

RCs 4–10 are shown in Fig. 7(c and d). The vertical axis shows standardized reconstructed components.

The correlation function of the GSL with each atmospheric index in these reconstructed series is summarized in Fig. 8. From Fig. 8 we see that there are periodic relationships between the GSL RC 4–10 series and the RC 4–10 series corresponding to each of the atmospheric indices. The highest correlations (approximately 0.35 in absolute value) of GSL with SOI, PNA, and CNP for the RCs occurs at lags of approximately ±40 and ±58. The peaks/valleys of the GSL-SOI cross correlation function for the reconstructed series are approximately 30–35 months apart.

We estimated the coherence and phases among the reconstructed series using GSL as reference. A representative plot (GSL-SOI) of this analysis is presented in Fig. 9. There is significant coherence across the sum of RC 4–10 in essentially the same frequency bands that were found to have significant power by the MTM analysis of the raw series (Fig. 4). In addition, there is significant coherence for GSL-SOI at a period around 11 years. This is also indicated by the 116 month lag between the peaks in the cross correlation function between GSL and SOI.

The phase information in Fig. 9 is interesting. The phase difference between the two series is small in the 2 year and 5 year bands, while the series are essentially out of phase in the 3 year and decadal bands. Phase relationships for the CNP and (-PNA) reconstructed series also show this. Looking back at Fig. 7, we observe that there appears to be some slow drift in phase between the reconstructed GSL and SOI series, and the GSL and CNP (and PNA) series [Fig. 7(a, c, and d)]. This

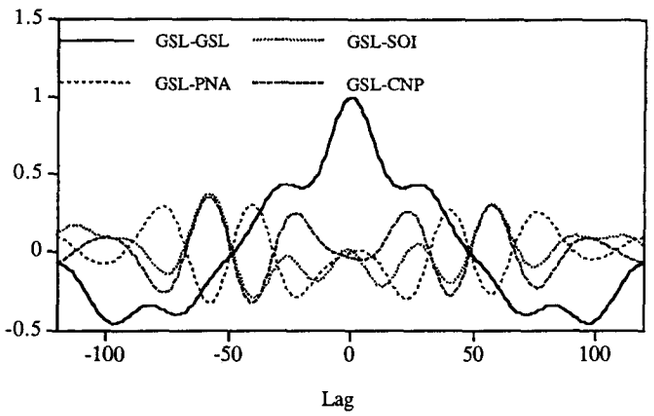

FIG. 8. Cross-Correlation Function of GSL with Sums of RCs 4–10 of Each Atmospheric Index

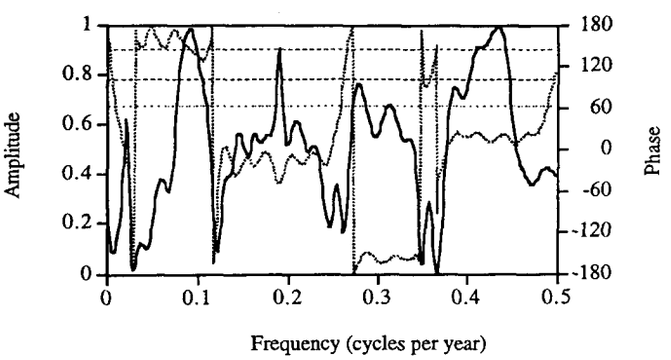

FIG. 9. MTM Coherence (Solid) and Phase (Dots) between GSL RC 4–10 and SOI RC 4–10, Using Three 2π Tapers. Coherence is Consistent with That Observed from Analysis of Raw Series (Fig. 4) at Frequencies around 0.4, 0.33, and 0.08. Dashed Lines Represent 90%, 95%, and 99% Significance Levels for Coherence

drift may be due to the mixing of signals within the resolution of the frequency analysis performed here.

CONCLUSIONS

We investigated low frequency connections between the GSL and three atmospheric circulation indices. First, the full (1847–1993) GSL time series was analyzed directly by SSA, to see if there was evidence of low frequency (interannual and interdecadal) variability. This analysis revealed "signals" in the 2.5–4 and 12–14 year frequency bands. The reconstructed components associated with these signals captured half the variability in a 12 month moving average of the GSL series. Pairwise MTM estimates of spectral coherence between the GSL and each atmospheric index using the much shorter (typically about 50 years) common records were showed commonalties in behavior at least at some frequencies. This analysis suggested coherence between the GSL and the SOI in the 2–4 year, 8 year, and 12 year frequency bands, and between GSL and PNA/CNP in the 2–4 year band. Finally, we investigated the common modes of variability in the GSL and the atmospheric indices using MSSA. This analysis confirmed the earlier results, lending confidence to the conclusion that the oscillatory patterns identified are common modes of atmospheric and GSL variation.

Lall and Mann (1995) argue that oscillations such as the ones reported here need to be interpreted carefully. It is unlikely that the identified "signals" represent strict periodicities in the climate system. However, they may represent unstable oscillatory modes that arise from nonlinear interactions between the ocean and atmospheric circulations. Some such oscillations may be self sustained, while others may be forced by anomalous events. Burroughs (1992) notes that "cycles" identified in weather are wont to disappear soon after they have been reliably established. We have observed from analyzing a number of hydroclimatic time series, that while oscillations identified by spectral analysis methods can be both phase coherent and spatially coherent across series, sometimes the phase information is lost upon passage of the cycle through zero amplitude. Such events where the oscillation is interrupted (or phase information) is lost are nevertheless spatially coherent, suggesting that the observed behavior may indeed be real, and reflective of the nonlinear dynamics of the overall system.

Correlative analyses such as those presented here are useful in two ways. First, they stimulate useful directions of inquiry in developing physical or conceptual explanations for the mechanisms responsible for any structured behavior that is identified. Second, they are useful for designing better statistical forecasting models for hydrologic processes through the suggestion of causative factors and associated information sources. Current work is exploring both these directions.

Mechanistic explanations for the low-frequency behavior are being developed through a study of the nature of ocean-atmosphere interactions, specifically in the North Pacific, North Atlantic, and the tropics. The nature of the tropical El Niño variability was discussed earlier. Weaver et al. (1991), among others, have focused on anomalies in freshwater inflows in the Greenland Sea as a trigger for internal oscillations in the North Atlantic thermohaline ocean circulation, which subsequently appears to affect atmospheric circulation at a decadal time scale through changes in the surface heat fluxes. The interaction of the subtropical North Pacific ocean circulation with the Aleutian low pressure system centered in the Arctic region of the North Pacific, and the possible poleward transport of heat in the ocean at interannual time scales are also cited (e.g. Latif and Barnett 1994) as possible factors in generating the observed low-frequency climatic variability in continental records. This is an active area of research into a complex puzzle, where a number of interacting mechanisms involving the ocean, the atmosphere and orographic and continental factors (e.g., soil moisture and vegetative state) play a role at a variety of time scales.

Lall et al. (1995) demonstrated considerable skill in forecasting the GSL, using a nonparametric approach that is based on ideas from nonlinear dynamical systems. This forecasting skill reflects an ability to exploit low-frequency oscillatory components, such as those identified here, for enhanced predictability at times other than when the system goes through a regime or phase shift. We are extending this approach for forecasting the GSL volume using time series of the GSL volume and the atmospheric indices. Locally weighted polynomials with automatically chosen order, number of neighbors, and embedding parameters are being used to develop the nonlinear forecasting model.

ACKNOWLEDGMENTS

Partial support of this work by the USGS Grant No. 1434-92-G-226 and NSF Grant No. EAR-9205727 is acknowledged. We thank D. R. Cayan for providing the atmospheric data and Scott D. Bartholoma for GSL data. We are also grateful for MTM codes and comments by M. Mann.

APPENDIX. REFERENCES

Barnston, A. G., and Livezey, R. E. (1987). "Classification, seasonality and persistence of low-frequency atmospheric circulation patterns." *Monthly Weather Rev.*, 115, 1083–1126.

Burroughs, W. J. (1992). *Weather cycles: real or imaginary?* Cambridge University Press, New York, N.Y.

Cayan, D. R., and Peterson, D. H. (1989). "The influence of North Pacific atmospheric circulation on streamflow in the west." *Aspects of climate variability in the Pacific and Western Americas*. American Geophysical Union, Washington, D.C.

Cayan, D. R., and Roads, J. O. (1984). "Local relationships between United States West Coast precipitation and monthly mean circulation parameters." *Monthly Weather Rev.*, 112, 1276–1282.

Cayan, D. R., and Webb, R. H. (1992). *El Nino, historical and paleoclimatic aspects of the southern oscillation*, Cambridge University Press, New York, N.Y.

Dettinger, M. D., and Ghil, M. (1991). "Interannual and interdecadal variability of surface-air temperatures in the United States." *Proc. XVIth Annu. Climate Diagnostics Workshop*, U.S. Department of Commerce, NOAA, Los Angeles, Calif., 209–214.

Emery, W. J., and Hamilton, K. (1985). "Atmospheric forcing of interannual variability in the northeast Pacific Ocean: connections with El Nino." *J. Geophysical Res.*, 90, 857–868.

Ghil, M., and Vautard, R. (1991). "Interdecadal oscillations and the warming trend in global temperature time series." *Nature*, 350, 324–327.

Hirschboeck, K. K. (1987). "Hydroclimatically-defined mixed distributions in partial duration flood series." *Hydrologic Frequency Modeling*, D. Reidel Publ. Co., Dordrecht, The Netherlands.

Horel, J. D., and Wallace, J. M. (1981). "Planetary scale atmospheric phenomena associated with the southern oscillation." *Monthly Weather Rev.*, 109, 813–829.

Keppenne, C. L., and Ghil, M. (1992). "Adaptive filtering and prediction of the southern oscillation index." *J. Geophysical Res.*, 97, 20449–20454.

Kiladis, G. N., and Diaz, H. F. (1989). "Global climatic anomalies associated with extremes in the southern oscillation." *J. Climate*, 2, 1069–1090.

Klein, W. H. (1985). "Space and time variations in specifying monthly mean surface temperatures from the 700 mb height field." *Monthly Weather Rev.*, 113, 277–290.

Klein, W. H., and Bloom, H. J. (1987). "Specification of monthly precipitation over the United States from the surrounding 700 mb height field." *Monthly Weather Rev.*, 115, 2118–2132.

Lall, U., and Mann, M. E. (1995). "The Great Salt Lake: a barometer of low frequency climatic variability." *Water Resour. Res.*, 31(10), 2503–2516.

Lall, U., Sangoyomi, T., and Abarbanel, H. D. I. (1995). "Nonlinear dynamics of the Great Salt Lake: nonparametric short term forecasting." *Water Resour. Res.*, 32(4).

Latif, M., and Barnett, T. P. (1994). "Caused of decadal climate variability over the North Pacific and North America." *Sci.*, 266, 634–637.

Leathers, D. J., Yarnal, B., and Palecki, M. (1991). "The Pacific/North American teleconnection pattern and United States climate. part I: regional temperature and precipitation associations." *J. Climate and Appl. Meteorology*, 24, 463–471.
Lins, H. F. (1993). "Seasonal hydrology variability and relations with climate," PhD dissertation, Univ. of Virginia, Reston, Va.
Lorenz, E. N. (1990). "Can chaos and intransitivity lead to interannual variability?" *Tellus*, 42A, 378–389.
Mann, M. E., Lall, U., and Saltzman, B. (1995). "Low frequency climate variability: understanding the rise and fall of the Great Salt Lake." *Geophysical Res., Letters*, 22, 937–940.
Mann, M. E., and Park, J. (1993). "Spatial correlations of interdecadal variation in global surface temperatures." *Geophys. Res. Letters*, 20, 1055–1058.
Mann, M. E., and Park, J. (1994). "Global-scale modes of surface temperature variability on interannual to century timescales." *J. Geophys. Res.*, 99, 25819–25833.
Namias, J. (1978). "Multiple causes of the North American abnormal winter 1976–77." *Monthly Weather Rev.*, 106, 279–295.
Preisendorfer, R. W. (1988). *Principal component analysis in meteorology and oceanography*. Elsevier Science Publishers, New York, N.Y.
Ropelewski, C. F., and Halpert, M. S. (1987). "Global and regional scale precipitation patterns associated with the El Nino/southern oscillation." *Monthly Weather Rev.*, 115, 1606–1626.
Sangoyomi, T. B. (1993). "Climatic variability and dynamics of Great Salt Lake hydrology," PhD dissertation, Utah State Univ., Logan, Utah.
Thomson, D. J. (1982). "Spectrum estimation and harmonic analysis." *IEEE Proc.*, 70, 1055–1096.
Trenberth, K. E., and Shin, W.-T. (1984). "Quasi-biennial fluctuations in sea level pressures over the Northern Hemisphere." *Monthly Weather Rev.*, 112, 761–777.
Vautard, R., and Ghil, M. (1989). "Singular spectrum analysis in nonlinear dynamics, with applications to paleoclimatic time series." *Physica D*, 35, 395–424.
Vautard, R., Yiou, P., and Ghil, M. (1992). "Singular-spectrum analysis: a toolkit for short, noisy chaotic signals." *Physica D*, 58, 95–126.
Vernon, F. L., Fletcher, J., Chave, A., and Sembrera, E. (1991). "Coherence of seismic body waves from local events as measured by a small-aperture array." *J. Geophys. Res.*, 96, 11981–11996.
Weare, B., and Nasstrom, J. S. (1982). "Examples of extended EOF analysis." *Monthly Weather Rev.*, 110, 481–485.
Weaver, A. J., Sarachik, E. S., and Marotze, J. (1991). "Freshwater flux forcing of decadal and interdecadal oceanic variability." *Nature*, 353, 836–838.